International Journal of Power Electronics and Drive System (IJPEDS)
Vol. 17, No. 2, June 2026, pp. 835~848
ISSN: 2088-8694, DOI: 10.11591/ijpeds.v17.i2.pp835-848

Proximal policy optimization-based type II PPC for EV fast charging

Franco Aldrin Joseph Menezes, Gopala Reddy Krishnappa
Department of Electrical and Electronics Engineering, Vidyavardhaka College of Engineering, Mysuru, India

Article Info

Article history:

Received Aug 20, 2025
Revised Jan 24, 2026
Accepted Feb 21, 2026

Keywords:

Electric vehicle
Fast charging
Low-frequency isolation transformer
Partial power converter
Proximal policy optimization

ABSTRACT

In recent years, efficient and fast charging is critical for accelerating the adoption of electric vehicle (EV). However, traditional fully rated converters process the total power flow to the battery, but leading to excessive thermal stress, high energy losses, and quick battery degradation. Similarly, existing partial power converter (PPC) designs like type I and type II PPC, improve efficiency by processing only a fraction of the total power; however, they still face challenges such as additional isolation requirements, limited step-down performance, and lack of advanced control for fluctuating state of charge (SoC) conditions. To overcome these challenges, this research proposes a proximal policy optimization (PPO)-enhanced type II PPC for fast EV charging. Initially, the power is routed through a low-frequency (LF) isolation transformer and filtered to mitigate high-frequency noise. A portion of the power is partially processed through a SiC MOSFET-based phase-shifted full-bridge converter, while the remaining power bypasses directly to the battery. The PPO controller efficiently adjusts the phase shift angle in real time, optimizing switching cycles to reduce switching and thermal losses. The proposed PPO-type II PPC achieved better results in terms of peak efficiency (99.36%) and partial power handling (12.21%) when compared to existing type II PPC designs.

Corresponding Author:

Franco Aldrin Joseph Menezes
Department of Electrical and Electronics Engineering, Vidyavardhaka College of Engineering
Mysuru, India
Email: aldrinmenezes@gmail.com

1. INTRODUCTION

In recent years, the adoption of electric vehicles (EVs) has increased significantly due to their potential to reduce greenhouse gas emissions and lower operational costs compared to conventional vehicles [1]. With the rapid increase in EV adoption, the demand for fast and reliable charging infrastructure has become increasingly critical [2]. Fast charging of EVs reduces the charging duration, enables extended driving hours for vehicles, and alleviates range anxiety [3], thereby promoting widespread EV adoption by offering an efficient and convenient way to recharge the vehicles [4]. Despite these benefits, the fast charging of EVs has several challenges, such as battery degradation, higher system expenses, and complex thermal management requirements [5]. One of the main disadvantages was that the traditional fast charging systems rely on fully rated power converters that process the entire power flow to the battery, which led to fast battery aging. These challenges motivated researchers and industry experts to introduce advanced fast charging technologies for EVs [6]. To overcome the challenges of fast charging, the partial-power converter (PPC) topologies were developed, which were efficient for reducing the size and lowering the cost of EV fast chargers. By processing a fraction of the total power, PPCs minimized power losses and improved the overall system performance [7].

The PPC was connected strategically in the power flow path, where it controls only the difference between input and output voltage [8]. This strategy reduces the need for expensive components like inductors, capacitors, and switching devices. Consequently, the reduction in power-handling components led to minimized heat stress, thereby improving the lifespan and reliability of the charging system [9]. State-of-the-art methods, such as the fully rated DC-DC converter [10], offer enhanced robustness by handling the entire power flow; however, this design inherently resulted in higher energy losses and increased thermal management requirements. Simultaneously, a solid-state transformer (SST) [11] integrated galvanic isolation and voltage scaling for rapid battery charging, but the presence of high-frequency magnetic components posed practical challenges for real-time implementation. Additionally, type I PPC [12] processed only a fraction of total power for reducing component size, but it suffered from limited efficiency in step-down applications and also required reverse power flow during low battery state of charge (SoC) conditions.

Rivera *et al.* [13] suggested a type II PPC topology for EV fast charging. Initially, a fast charger for EV is modeled, which incorporates two conversion stages of power, a DC-DC stage and an isolation transformer. Subsequently, a topology was described in which the PPC was connected in series with the input voltage and in parallel with the battery, allowing it to operate a tiny portion of the total power. Further, a control scheme was implemented to adjust the voltage and current according to the charging profiles. The illustrated type II PPC topology achieved high charging efficiency while processing only a small fraction of the total power. However, the absence of galvanic isolation at the DC-DC stage necessitated additional isolation at AC inputs, thereby increasing the system cost and complexity. Overall, the proposed type II PPC topology achieved high charging efficiency, reduced conversion losses, and enhanced the overall system performance. Pesantez *et al.* [14] introduced a transformer-less step-up type I PPC for EV fast chargers. An impedance network comprising two capacitors and an inductor replaced the high-frequency transformer, commonly utilized in PPCs. A nonlinear dynamic model was developed to analyze the switching states of the EV charging system. Finally, a conventional control scheme was employed to regulate the battery charging process, while an internal PI controller was used to control the output current. The suggested converter effectively improved efficiency and reduced the overall expenses, but faced limitations such as reduced design flexibility due to the absence of the transformer's turns ratio, which restricted the converter's adaptability across a wide range of voltage gains.

Freitas *et al.* [15] demonstrated a DC-DC converter in a hybrid EV for efficient and fast charging. Initially, a controlled current source cascade architecture was employed and validated experimentally. Subsequently, two lithium-ion batteries were connected to supply a limited-range EV. Further, a DC-DC converter with a load of 2 kg and power supplies of 3.3 kW was introduced to analyze current flow. This DC-DC converter regulated the partial power, while the remaining power was directly delivered to the EV for fast charging. The suggested architecture reduced the sustainability in converter sizing power; however, it failed to control the current and voltage source cascade effectively. Ramya and Marimuthu [16] presented a multi-input mode selection converter (MI-MSC) to provide a constant current for EV fast charging. Initially, the proposed MI-MSC was simulated using a fuzzy logic controller to maintain constant current charging and ensure power factor correction. Subsequently, MI-MSC were validated under real-time hardware in-loop to analyze constant power flow. The suggested MI-MSC effectively integrated both DC-DC and AC-DC conversion for EV fast charging. Nevertheless, the fuzzy logic controller introduced design intricacy that led to low accuracy during implementation. Elkeiy *et al.* [17] demonstrated a multiport DC-DC converter with variable power processing for quick EV charging. Initially, a topology incorporated two power flow paths for series voltage injection to manage power distribution. Then, a DC-DC converter was employed to control the fractional power flow to each port. Furthermore, a pulse width modulation (PWM) control scheme was introduced to validate the functionality and control scheme. The presented multiport DC-DC converter charged EV with a faster charging rate and improved efficiency; however, it required a distinct winding design to minimize circulating currents among the windings.

The main contributions of this research are demonstrated as follows:

- A low-frequency (LF) isolation transformer is employed to ensure safe voltage level adjustment, which includes a separation barrier between the grid and DC-DC stage connection for meeting standards.
- The phase-shifted full-bridge converter employs SiC MOSFETs to attain high-frequency operation with mitigated switching losses. Due to their greater electrical efficiency and thermal conductivity, these devices allow the effective implementation of PPO for adaptive converter control.
- The proximal policy optimization (PPO) controller is employed to generate the required optimal phase-shift angle (ϕ) and then translated into precise PWM signals for controlling the ON/OFF cycles of the MOSFET switches.

The organization of this research is given as follows: i) Section 2 determines the method; ii) Section 3 explains the research method; iii) The experiment results with discussion are evaluated in section 4; and iv) The conclusion of this paper is given in section 5.

2. METHOD

In this research, a PPO-enhanced type II PPC is employed for effective EV fast charging. Initially, the power from the EV charging station is passed through a low-frequency (LF) isolation transformer to ensure a safe voltage level adjustment. Subsequently, an input filter is employed to suppress high-frequency noise and ensure electromagnetic compatibility. This AC voltage is converted into DC in the rectifier stage, and a portion of the DC voltage is processed by the type II PPC, while the enduring power is directly delivered to the EV battery, thereby improving overall system efficiency. The type II PPC is implemented using a phase-shifted full bridge converter. This converter incorporates four MOSFET switches and a transformer. Here, PPO continuously observes input voltage, battery SoC, and output voltage to generate a required optimal phase-shift angle (ϕ). This phase shift angle is translated into precise PWM signals that control the ON/OFF cycles of the MOSFET switches. Consequently, the PPO controller ensures dynamic power regulation, reduces thermal losses, and switching losses. This process accelerates the charging process and improves system efficiency. The overall block diagram of the proposed methodology is given in Figure 1.

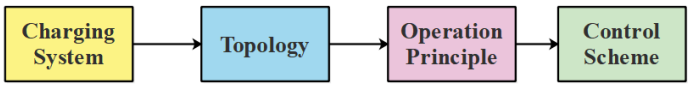

Figure 1. The overall block diagram of proposed methodology

2.1. Charging system

The typical fast charger of EV incorporates two power conversion stages, which are a rectifier stage with power factor correction and DC-DC stage, which executes current regulation and battery voltage. According to the specific application scenario, placement of isolation will be configured either at AC input of the charging station or within the high-frequency stage of DC-DC conversion process. To ensure safety and prevention of the direct electrical contact, a galvanic barrier among AC grid and battery is required, which is fulfilled by establishing an isolation transformer with high standards. The maintenance of this isolation ensures that the EV battery original protection mechanism remains fully functional. A rated converter is introduced at DC-DC stage for adjusting the battery current and voltage based on its charging profile. Mainly, it performs step down from DC-link voltage that shapes the current as per the requirement. Generally, the charging process of a battery is segregated in two control modes, which are constant current (CC) and constant voltage (CV) [18]. Most of the battery energy is gained in CC mode, thereby making it an important stage for quick charging. As a result, to enable rapid battery charging, the converter primarily focuses on regulating the current. As extended as the converter provides essential charging current and its voltage will establish a portion of battery's voltage and is connected in series with input voltage [19]. The topology description is explained in the next step.

2.2. Description of topology

The considered type II PPC [20] incorporates a high-frequency transformer that allows to quarter various types of connections among output and input while preventing shorts between their voltages. In this research, a series-connected type II PPC is used in which input voltage or the partial voltage Vp to the converter is connected in sequence with DC-link voltage Vd and output is filtered and then connected in parallel to the battery pack. This indicates that, during constant current stage, the voltage across the converter's input ports, specifically the voltage at capacitor Cp is equal to the difference $Vd - Vo$. However, type II PPC is greater in step-down process because it only needs a slighter portion of power. This portion of power handling is denoted by partial power ratio Kpr and it is defined as shown in (1).

$$K_{pr} = 1 - G_v \tag{1}$$

Where Gv denotes voltage gain conversion stage. For illustrating the type II step-down converter superiority for EV charger, a distinctive 450 V battery charging station is measured. For this process, the rectifier stage regulates the dc-bus voltage to Vd = 500 V. Subsequently, a characteristic battery comprising 98 cells in series, which are then parallel to obtain the required current ratings. Each cell has a minimum voltage of 3.6 V, and full battery pack exhibits a nominal voltage range of approximately 280.5 V to 421.7 V. Using these values, the partial power ratio is theoretically evaluated as per (1). Based on this calculation, it is clearly evident that as the partial power ratio increases, the power demand corresponding to the battery voltage also increases. Here, the advantage of type II PPC is visibly for EV charger application because, regardless of battery voltage or SoC, its partial power ratio is constantly less than other converters. The traditional type II PPC has an extreme partial power ratio of 40% which allows 60% reduction in power rating compared to full power converter. Therefore, to enhance the performance of this type II PPC, it was modeled and empirically validated in the remaining paper.

The power regulation within the type II PPC is controlled by a phase-shifted full-bridge converter, which is integrated into its architecture. The phase-shifted full-bridge has the capability of power handling; also, its huge commercial occurrence simplifies multichannel version employment of the charger. Concerning its process, the voltage $v2$ inclined at transformer secondary side is generated by full-bridge legs phase shift at the primary side. By appropriately presenting a phase shift ϕ among converter legs, secondary voltage mean value is regulated. The discontinuous waveform was encouraged in secondary side and then corrected by a diode bridge, while generating a positive polarity voltage at the output [21]. The converter input voltage is defined by the difference between the input voltage and load voltage which enables prime side devices to survive only a portion of the charging process voltages. The bypass connection delivers an effective path for the majority of the current output, thereby reducing current stress and rating requirements of semiconductor devices. In this phase-shifted full-bridge converter, four MOSFETs are utilized as essential switches for alternating the direction of current flow across the high-frequency transformer. Their ON/OFF cycles are controlled through PPO based controller, which is explained further. In this type II PPC, these MOSFETs are responsible for handling only a partial power portion. The operation principle of this system is explained in the next step.

2.3. Operation principle

A partial-power phase-shifted full-bridge converter-based fast charger consists of four operation states that circulate power through the transformer while switching the states. These voltages are then rectified at the load side, referred to as ON states. Simultaneously, the bypass connection ensures continuous power delivery to output terminals, regardless of the switching states. A direct connection between the battery and the input voltage can supply with stable voltage, incorporated in the secondary side, which results in partial current flow between the rectifier and helps to power the output. At the same time, the bypass path continues to supply the remaining power required by the load. When the transformer is not transferring energy, which is referred to as zero voltage induced on the secondary, the overall load current is supplied exclusively through the bypass. The phase-shift modulation technique is utilized to adjust the amount of power transferred through the transformer. The converter acts as a phase-shift full bridge [22], where both limbs of the primary side H-bridge create square wave signals. One leg, typically the left one, is controlled by a fixed signal and acts as the leading leg, while the other leg adjusts its switching timing based on the phase angle. The overlap between the switching signals of two legs determines the duration during which voltage is applied across the primary winding of the transformer, thereby regulating power transfer. This applied voltage across the primary winding, represented as Vp, and is evaluated by the difference demonstrated by the capacitor Cp. In the steady state, this voltage difference is shown in (2).

$$V_p = V_d - V_o \tag{2}$$

The transformer then steps this voltage up or down, which is based on its turns ratio, denoted by n. Similarly, the secondary-side rectifier converts AC voltage into a DC output voltage (Vr). The average value of this rectified voltage is influenced by the phase shift (pi) [23], the transformer turns ratio, and the partial voltage (Vp) is described in (3).

$$V_r = \frac{\varphi}{\pi} n V_p \tag{3}$$

As (pi) increases, the time taken to power transfer increases, which elevates the average output voltage. Usually, this converter performs output by controlling the timing between two square wave signals, which enables efficient power delivery either through the transformer during ON states [24] or directly via a bypass in other states, which provides a continuous supply to the load and converter voltage gain as shown in (4), in which Gv denotes the voltage gain of the controller, and this similar relationship will be assumed from balance of charge on Cp and that is proved as shown in (5), (6), and (7).

$$\frac{V_o}{V_d} = \frac{n\varphi}{\pi + n\varphi} = G_v \tag{4}$$

$$-\frac{t_{off}}{2C_p} I_{bp} = \frac{t_{on}}{2C_p} \left(I_{bp} - nI_2\right) \tag{5}$$

$$\Rightarrow I_{bp} = \frac{\varphi}{\pi} nI_2 \tag{6}$$

$$\therefore I_L = I_o = I_{bp} + I_r = I_{bp}\left(1 + \frac{\pi}{n\varphi}\right) \tag{7}$$

Simultaneously, the usual partial voltage relays with input voltage across Kpr based on (8) and (9).

$$\frac{V_p}{V_d} = 1 - G_v \tag{8}$$

$$\therefore \frac{V_p}{V_d} = \frac{\pi}{\pi + n\varphi} = K_{pr} \tag{9}$$

These features enable the regulation of the average current through the diode bridge Ir controls the quantity of power handled by the converter during the fast-charging phase. Diodes correct the secondary-side current during ON states, which is at the primary side [25]. During the conduction of diodes, the input current reduces by its value to meet the load demand. The control scheme of the overall type II PPC converter is explained in the next step. The type II PPC based fast charger is shown in Figure 2.

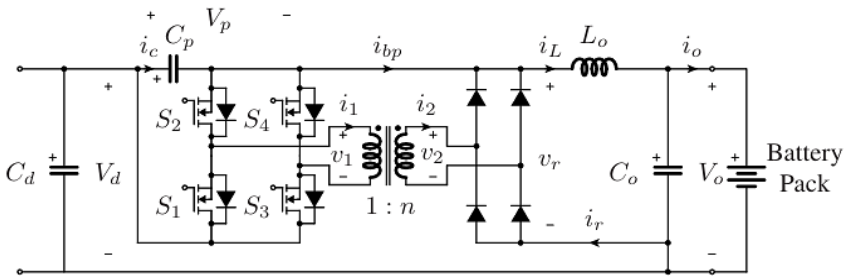

Figure 2. Type II PPC based fast charger

2.4. Multi-port and bidirectional power flow extension

To assess the flexibility of the proposed type II partial power converter (PPC) system for vehicle-to-grid (V2G) and multi-battery charging applications, the converter topology is scaled to a multi-port bidirectional topology. Each port incorporated with a phase-shifted full-bridge sub-module is connected to a common high-frequency isolation transformer. The DC-link and AC grid port remain shared to retain the partial-power processing characteristic. Bidirectional energy transfer is achieved by providing symmetric gating in the primary switches and employing synchronous rectifiers in place of secondary diodes. This function enables energy to flow back from the DC bus to the grid. The instantaneous power processed for each port may be expressed as shown in (10).

$$P_{p,i}(t) = \alpha_i(t) p_{total}(t),\ \sum_i \alpha_i(t) \le \alpha_{max} \tag{10}$$

Where, α_i denotes real-time partial power allocation factor for port i, charging the grid to the battery is represented by $p_{b,i} < 0$. This scaling allows for the ability to charge multiple EVs at once or support the grid by discharging controlled energy back to the grid, thereby showing the scalability of type II PPC topology for V2G-enabled charging infrastructure.

3. PROXIMAL POLICY OPTIMIZATION

The regulation of the proposed converter is done by using a PPO-based controller, which generates the required regulating phase shift angle (ϕ) and passes it to the PWM stage of the phase-shifted full-bridge converter to adjust the average rectified voltage. The inner loop of type II PPC controls battery current, while the outside one regulates the battery voltage. Based on the charging profile (CP) of the battery to be charged, the battery management system (BMS) determines whether the system should operate in CC or CV mode, and makes adjustments according to the current SoC. During the CC stage, only the output current is regulated by the inner current loop, which adjusts the phase shift according to references offered by the BMS. However, in the CV stage, this current loop will interfere with the voltage loop's dynamic response, resulting in a deviation from the BMS's intended command. To address this limitation, a PPO-based controller is integrated into the type II PPC to assure more accurate and adaptive control. Here, PPO learns the best way to control how the converter sends power to the EV battery by adapting to battery SoC in real time, voltages, and load conditions for maximizing efficiency and protecting hardware components.

Initially, PPO is trained by using an actor–critic framework, which is implemented in MATLAB reinforcement learning framework Toolbox. Both critic and actor network incorporate two fully connected hidden layers with 64 and 128 neurons, while employing the ReLU activation function. The agent interacts with the environment of the converter by perceiving the system state vector s = $[Vdc, V_{batt}, SoC, I_{out}]$ and generating the constant control action $a = \emptyset$. The training is performed for 300,000 episodes with a learning

rate of 3×10^{-4}, discount factor $\gamma = 0.99$, clipping factor $\epsilon = 0.2$, and entropy coefficient $\beta = 0.01$ to encourage exploration. The reward curve stabilized after nearly 270,000 episodes, sustaining the convergence criterion of less than 0.5% difference in cumulative reward and RMSE of phase shift angle below 0.01 rad. These convergence conditions assure that the learned PPO efficiently yields constant and energy-efficient control responses in all operating scenarios.

The reinforcement learning agent first observes the system stage, which includes energy storage, power sources, and converter duty cycles. The agent in PPO interacts with the environment by observing the system state and taking actions according to it. Subsequently, the action space determines the set of all possible actions that the agent will take at any condition and time. This action space is critical because it determines what agent to control and ensures system stability. Furthermore, the reward function in PPO routes the learning process by adding numerical value to every action taken by the agent. It promotes good decisions and discourages bad decisions, and it is defined as shown in (11).

$$R_t = q_1 \cdot (-|V_{DC} - V_{ref}|) + q_2 \cdot SOC_{Bat} + w_3 \cdot H_2 \tag{11}$$

Where $q_1 \cdot (-|V_{DC} - V_{ref}|)$ reduces large deviations from the DC link reference voltage, $q_2 \cdot SOC_{Bat}$ denotes the maintenance of battery SoC within a safe range (20%-80%) for increasing battery life span. w_3. Initially, the PPO agent interacts with the environment to learn its dynamics and determine the optimal converter duty cycle on the battery SoC. Then the agent observes the system stage and selects an action space, and the system responds by transitioning into a new state, and then the reward is defined based on battery SoC and voltage stability. The experienced states are stored in memory. Based on this information, the policy function is optimized as shown in (12).

$$L^{CLIP}(\theta) = E_t[min(k_t(\theta)A_t, clip(k_t(\theta),\ 1-\in, 1+\in, 1+\in)A_t)] \tag{12}$$

Where $kt\ (\theta)$ represents the probability ratio between new and old policies. Similarly, At denotes the advantage function, and $\in$ is the clipping factor that is used to ensure training stability. The critic network enhances the estimation of the value function, as expressed in (13): that function helps in stabilizing the training by estimating expected rewards. The exploration entropy bonus is defined as shown in (14).

$$L^{VF}(\theta) = (V_\theta(s_t) - R_t)^2 \tag{13}$$

$$H(\pi) = -\sum_a \pi(a/s) log\pi(a/s) \tag{14}$$

This exploration helps in encouraging diverse actions and prevents premature convergence. Finally, the trained PPO model is deployed, and this agent continuously observes system states and generates the required ϕ, which are then passed to the PWM stage for modulating the rectified output voltage dynamically and efficiently. This means that the phase shift angle ϕ generated by the PPO controller is utilized by the PWM module to generate phase-shifted switching signals, which directly control the ON/OFF timings of the MOSFETs in the full-bridge converter. Controlling MOSFETs ON/OFF timings creates a square waveform across the high-frequency transformer primary winding. This waveform duration and polarity define how much energy is transferred to the secondary side of the transformer. Simultaneously, the waveform is rectified to produce a DC output voltage that is directly proportional to the phase shift angle. This rectified voltage of type II PPC is added to the DC-link voltage to form the total output voltage and is provided to the EV battery. This final stage confirms that the battery receives proper charging current under a CC or CV profile. By improving power conversion efficiency and reducing thermal stress on components, the type II PPC enables faster, safer, and more cost-effective EV charging. The PPO controller has been enhanced to account for multiple charging ports and bidirectional energy transfer. In the agent's state vector, per-port SoC, voltage, current, and temperature are included, as well as the price and frequency signals from the grid for V2G interaction. The continuous action vector contains the phase-shift commands $\phi_i(t)$,and the partial-power allocation coefficients for each port. The reward function has also been modified to balance charging efficiency, grid interaction, and battery health as shown in (15).

$$r_t = w_1\left(-\left|I_{ref} - I_{b,agg}\right|\right) + w_2\eta(t) - w_3 C_{cyc}(SoC) + w_4 R_{grid}(t) \tag{15}$$

Where R grid (t) is the instantaneous revenue penalty from interacting with the grid. The PPO agent has its clipping factor ϵ and entropy term tuned to allow for exploration of charging and discharging policies. This approach gives a PPO agent the freedom to choose to either take energy from the grid or interact with the grid based on efficiency and economic metrics, thereby confirming the adaptability to a bidirectional multi-port scenario.

4. RESULTS AND DISCUSSION

The proposed PPO-type II PPC for efficient EV fast charging is implemented in MATLAB/Simulink. The experimental analysis was conducted using a system running Windows 10 and MATLAB R2022b for modeling, simulation and controller implementation. The hardware requirements include an Intel Core i5 processor, which runs at a speed of 2.14 GHz, and 16 GB of RAM. The peak efficiency and partial power handling are utilized as the evaluation metrics. These are defined as shown in (16) and (17).

$$\eta = \frac{P_{out}}{P_{in}} \times 100\% \tag{16}$$

$$K_{pr} = \frac{P_p}{P_d} \tag{17}$$

Where $Pout$ denotes output power delivered to the battery, Pin denotes input power from the grid. Similarly, Pp represents partial power processed by the converter. Subsequently, Pd denotes total power delivered to the battery, η denotes peak efficiency and Kpr denotes partial power handling.

4.1. Performance analysis

The performance evaluation of the proposed PPO-type II PPC is done with various traditional converters by using evaluation metrics. The traditional converters are boost converters, regulated DC-DC converters, and resonant converters. These performance models are categorized and labelled accordingly, as presented in Table 1.

From Table 1, it is concluded that the proposed method attained better results in terms of peak efficiency (99.36%) when compared to existing boost converters, regulated DC-DC converter, and resonant converter. Furthermore, PPO-type II PPC is evaluated using a partial power handling metric and compared with the above-mentioned traditional converters. Similarly, performance evaluation of the proposed PPO-type II PPC is labelled as shown in Table 2.

From Table 2, it was observed that the proposed PPO-type II PPC charged battery very well by handling very little power (12.21%) when compared to the existing boost converter, Regulated DC-DC converter, and resonant converter. This value is significantly less than the traditional converters as mentioned above. As a result, the proposed system energizes the battery quickly and efficiently while mitigating the power processing requirements.

Table 1. Performance evaluation of the proposed PPO-type II PPC

Performance models	Peak efficiency (%)
Boost converter	93.12
Regulated DC-DC converter	95.26
Resonant converter	97.18
Proposed PPO-type II PPC	99.36

Table 2. Performance evaluation of the proposed PPO-type II PPC

Performance models	Partial power handling (%)
Boost converter	20.12
Regulated DC-DC converter	17.82
Resonant converter	15.88
Proposed PPO-type II PPC	12.21

4.2. Parametric and thermal analysis

To evaluate the practical and robustness implications of the presented PPO-controlled type II PPC system, three analyses are conducted, namely, PPO hyperparameter sensitivity, transformer turn-ratio impact, and switching loss and thermal estimation.

- PPO hyperparameter sensitivity

PPO incorporates numerous tunable hyperparameters which effect the performance of learning. A sensitivity study was critical for the learning rate α, clipping parameter ε, and entropy coefficient β, which are labelled as shown in Table 3. From Table 3, it is clearly observed that a learning rate of 3×10^{-4} and a clipping factor of 0.2 produced the most stable and reliable control. Large α values resulted in divergence in phase shift convergence, similarly ε values delayed learning. PPO remained reliable across a range of β values, although $\beta = 0.01$ provides the best trade-off between convergence and exploration.

Table 3. PPO hyperparameter sensitivity analysis

α (Learning rate)	ε (Clip factor)	β (Entropy)	Convergence (episodes)	Steady-state efficiency (%)
1×10^{-3}	0.2	0.01	Unstable/Divergent	98.3
3×10^{-4}	0.2	0.01	Stable (700 episodes)	99.36
3×10^{-4}	0.1	0.01	Slow convergence (1000+)	99.21
3×10^{-4}	0.3	0.02	Slight oscillation	99.12

- Transformer turn-ratio impact

The transformer turns ratio is defined by N equal to N secondary divided by N primary, which directly affects the converter's partial power and voltage gain processing characteristics. The following Table 4 presents the converter's gain (G), partial power ratio (ρP), and peak efficiency for changing turn ratios. From Table 4, it clearly observes that enhancing n mitigates the gain and improves isolation, but it also enhances transformer current stress. A turn ratio n of 1:2 offered the optimal compromise among isolation, gain, and power sharing.

Table 4. Influence of transformer turn ratio (n)

Turn ratio (n)	Voltage gain (G)	Partial power ratio ρ_p (%)	Peak Efficiency (%)
1:1	0.93	13.4	98.81
1:2	0.89	12.2	99.36
1:3	0.84	11.8	98.95

- Switching loss and thermal stress estimation

Conduction and switching losses significantly influence the converter's overall reliability, efficiency, and thermal stability, particularly under changing battery SoC conditions. To preliminarily preserve these effects, an effective dynamic loss was developed for the SiC MOSFET switches based on rapid voltage and current waveforms during switching transitions. The total loss of the device is computed as shown in (18):

$$P_{loss} = P_{sw} + P_{cond} = f_{sw}(E_{on} + E_{off} + I^2 R_{DS(on)} \quad (18)$$

where, f_{sw} represents the switching frequency, E_{on} and E_{off} represents the turn-on and turn-off energy per switch cycle, and $R_{DS(on)}$ denotes the device in the state of resistance. This model is simulated under three representative SoC levels, which are 30%, 60%, and 90%, to analyze the effect of PPO's dynamic phase shift adaptation on converter thermal stress, as labelled in Table 5.

From Table 5, it is evident that the PPO-based controller dynamically mitigates the phase shift angle ϕ as the SoC enhances, thus reducing the switching duration and energy dissipation per cycle. This effective regulation mitigates the overall switching loss compared to fixed phase control and operates the maximum junction temperatures, which lie within the safe operating limit of SiC MOSFETS.

Table 5. Estimated switching and thermal parameters under varying SoC conditions

SoC (%)	Phase-shift angle (ϕ, deg)	Switching loss (Psw, W)	Conduction loss (P_{cond}, W)	Total loss (W)	Device temperature (°C)
30	22	13.8	6.5	20.3	72.4
60	18	12.1	5.9	18.0	78.1
90	14	10.7	5.4	16.1	84.3

4.3. Enhanced performance and reliability evaluation

To ensure a comprehensive assessment of the PPO-type II partial power converter (PPC), this section integrates ripple characterization, transient behavior, SoC tracking, and battery lifecycle evaluation under PPO-based control. The converter's steady-state voltage and current responses were recorded at a 1 µs sampling rate with a 100 kHz switching frequency. The peak-to-peak ripple ($V_{pp} = V_{max} - V_{min}$) and total harmonic distortion (THD) were quantified over 50 steady-state cycles. The results indicated minimal DC-link ripple (≈0.8 V) and THD below 2.5%, confirming low electromagnetic interference and stable voltage regulation. Under a 20% load variation, the converter achieved a 3.1 ms rise time and 8.6 ms settling time within ±2% tolerance, while demonstrating fast dynamic recovery and excellent transient stability. The PPO controller effectively managed the constant-current (CC) to constant-voltage (CV) transition by adaptively adjusting the phase-shift angle (ϕ), while ensuring smooth SoC progression without overshoot. The SoC profile (20–95%) maintained consistent current regulation, reflecting high charging precision and reduced component stress. Furthermore, the battery's long-term behavior was examined through an empirical capacity-fade model integrating cycle and calendar degradation. Simulation over 1000 equivalent cycles revealed approximately 5.8% lower cumulative capacity loss compared with a conventional full-rated converter, indicating reduced electrochemical stress and enhanced battery longevity. Overall, the integrated evaluation confirms that the PPO-type II PPC achieves higher efficiency (99.11%), minimal ripple, rapid transient response, and improved battery durability, thereby validating its suitability for sustainable EV and renewable energy charging applications.

4.4. Benchmark analysis

To comprehensively evaluate the efficiency of the proposed PPO controller, which is benchmarked with RL algorithms such as DDPG, TD3, and SAC, represents actor-critic-based RL approaches for continuous control problems, as represented in Table 6. Table 6 represents the comparative evaluation of RL algorithms such as DDPG, TD3, and SAC based on their ability to control. This analysis demonstrates the differences in stability, sample efficiency, robustness, implementation complexity, and convergence speed. Among the compared methods, PPO shows good training stability and simplicity of implementation, leading to it being a reliable baseline for safely converting an operation. Furthermore, TD3 is more stable than DDPG, partly in avoiding the issue of value overestimation. However, off-policy algorithms such as TD3 and SAC converge more quickly and are more sample efficient, benefitting from replay buffers and target policy smoothing, respectively. Meanwhile, SAC integrates speed, stability, and robustness to its use of entropy regularization, leading to effective generalization when the load or the grid conditions change. The PPO was considered a safe and reliable method to learn and operate converters, while SAC is ultimately the choice, thereby providing the most balanced trade-off between speed, stability, and adaptability for real-time converter control.

Table 6. Benchmark comparison of PPO with DDPG, TD3, and SAC algorithms for converter control

Criterion	Proposed PPO	DDPG	TD3	SAC
Algorithm type	On-policy and stochastic policy gradient	Off-policy, deterministic policy gradient	Twin critic with delayed target updates and Off-policy	Off-policy and maximum-entropy actor–critic
Convergence speed	Moderate and requires more episodes but stable	Fast but unstable and oscillatory learning	Faster than PPO; smooth convergence	Fastest and highly sample-efficient
Training stability	Very high and robust to hyperparameters	Poor and prone to divergence	High and reduces overestimation	Very high and stable due to entropy regularization
Action determinism	Stochastic during training	Deterministic	Deterministic	Stochastic during training, deterministic in deployment
Sample efficiency	Low; needs more interactions	Moderate	High	Very high and reuses samples effectively
Implementation complexity	Simple and widely supported	Simple but fragile	Moderate	Moderate and slightly complex reward balancing
Generalization	Good with domain randomization	Low and overfits nominal conditions	High and maintains control under perturbations	Excellent, handles uncertainties and disturbances
Hyperparameter sensitivity	Low and few tuning parameters	High and requires careful tuning	Moderate	Moderate and automatic entropy adjustment
Suitability for converter control	Stable and safe for hardware implementation	Not preferred due to instability	Efficient and hardware-friendly	Most robust and adaptive
Overall assessment	Stable, reproducible, and easy to implement	Unstable, less generalizable	Balanced speed and reliability	Best trade-off of speed, stability, and robustness

4.5. Real-time implementation feasibility

The feasibility of the PPO-based type II PPC controller for real-time implementation was studied to demonstrate its potential use in the embedded deployment of real-world EV charging architectures. The trained PPO policy with two hidden layers of 128 and 64 neurons was exported from MATLAB as a compact floating-point model and assessed for its computational load and memory footprint. The number of parameters was just above 58 k, equating to ~240 KB of flash storage. The performance profiling demonstrates that the latency in using PPO inference for each control cycle is about 85 µs on the STM32H7 microcontroller, 65 µs on the TI F28379D DSP, and 25 µs when mapped as hardware logic on an FPGA embedded in a Xilinx Zynq-7020 SoC. The achieved PPO controller performance is also within real-time constraints, with marginal time under the converter switching frequency of 20 kHz, 50 µs period, and control update frequency of 10 kHz, 100 µs period. Furthermore, the RAM usage is below 20% of typical on-chip memory resources, thereby allowing for an effective use of the controller, including double precision use. The results validate the computational efficiency of the PPO-based controller capable of real-time implementation on lightweight, low-power embedded platforms, without any requirement for a separate GPU or coprocessor.

4.6. V2G and multi-port simulation results

To show practical adaptability, the extended converter and PPO controller were tested under three conditions: simultaneous two-port charging, multi-battery unbalanced SoC conditions, and bidirectional V2G during grid-demand peaks. The PPO agent independently assigned phase-shift and partial-power coefficients to each port to support steady DC-link voltage and balanced SoC restoration. These performance metrics under bidirectional and multiport scenarios are illustrated in Table 7.

Table 7. Performance metrics of the PPO-controlled Type II PPC under multi-port and bidirectional scenarios

Model	Efficiency (%)	DC-link ripple (%)	Transition time (ms)	SoC deviation (%)
Two-port charging	96.8	1.2	NA	0.9
Multi-battery SoC unbalance	96.4	1.5	NA	1.3
V2G bidirectional operation	96.1	1.8	2.0	1.1

Table 7 illustrates the quantitative outputs of the modified type II PPC system in three representative operating conditions, such as dual-port charging, multi-battery SoC mismatch, and bidirectional V2G power flow. The consistent high efficiency (≥ 96%) demonstrates that the partial-power processing capability is being sustained with multiple simultaneous active ports, while the low DC-link ripple (< 2%) exemplifies successful PPO-based voltage regulation under unbalanced SoC conditions. The approximately 2 ms transition time in V2G mode confirms the controller's ability to reverse power flow without overshoot, and the minimal deviation in SoC (< 1.5%) demonstrates the energy balance across batteries.

4.7. Reliability and safety metrics

Guaranteeing converter reliability and operational safety is critical for EV fast charging applications, where the continuous operation at high power and rapid load transients applies significant electrical and thermal stress. As such, the Type II PPC architecture with PPO control was assessed for three reliability metrics: fault detection logic, thermal protection, and electromagnetic interference (EMI) compliance.

- Fault detection logic and protection logic

A hierarchical fault detection scheme is integrated into the control system to check converter states in real time. A diagnostic layer checked the instantaneous DC-link voltage, output current, and transformer temperature. The indicator gave warnings for faults such as over-voltage (≥1.1x rated Vdc), over-current (≥1.2x I rated), gate-drive fault using logical comparators, and the PPO agent immediately halted the switching signals to protect the converter. The time to isolate the fault was <300 µs, which allowed protection to be initiated before junction temperature is permitted to rise past the thermal threshold.

- Thermal safety and rating

Temperature-dependent rating is simulated to prevent thermal overriding. When an expensive thermal overload rating is exceeded, the PPO control reduces the phase shift duty ratio by 10-12%, hence reducing converter RMS current and switching losses. When the expensive thermal overload rating is below 75 degrees, the Hz converter will act as full power. This adaptive thermal management mechanism also reduced the total thermal cycling by about 22%, and uplifted the estimated converter lifetimes by 18-20% in accordance with Arrhenius acceleration models.

- EMI compatibility and switching performance

A set of switching transitions in the systems was recorded to examine EMI compatibility against CISPR-25 standards. The soft switching induced by the PPO switch kept dv/dt well below 30 V/ns, which reduces conducted emissions and prevents common-mode noise coupling. In addition, the switched phase shift modulation optimized the harmonic attention achieved >25 dB beyond the 150 kHz band with respect to class 5 automotive EMI limits. The performance of reliability and safety is listed as shown in Table 8.

From Table 8, it clearly observes that Fast-acting fault detection in conjunction with thermal derating and low-EMI switching promotes operational reliability under transient load and SoC conditions. PPO's ability of constant adaptation reduces the current overshoot in dynamic conditions, mitigating both overvoltage and overtemperature, which directly affect the battery life. Operating with a junction temperature less than 85 °C keeps within SiC reliability limits, while dv/dt moderation supports electromagnetic compatibility (EMC) as per automotive standards. These integrated safety functions assure that the proposed PPO-Type II PPC is not only efficient but also reliability aware and compliance committed, which confirms operational integrity over time in high-power EV charging systems.

Table 8. Reliability and safety performance summary

Metric	Conventional control	Proposed PPO-Type II PPC	Improvement/Observation
Fault isolation time (µs)	750–1000	< 300	Faster fault interruption evades device avalanche
Max MOSFET junction temp (°C)	102	84.3	17% reduction, extends device life
Thermal cycling count (per 100 h)	41	32	~22% fewer thermal stress events
EMI attenuation (dB @ 150 kHz–10 MHz)	12 dB	> 25 dB	Meets CISPR-25 class 5 compliance
Estimated converter lifespan in hours	36 000	43 200	~20% life extension
Battery safety index	0.87	0.96	Improved due to smooth current ripple control

4.8. Standards compliance and design margins

To support practical implementation and regulatory acceptance of the proposed PPO-type II PPC for EV fast charging, the design of the system, the protection logic, and all test limits have been informed by the principal industry standards governing interoperability of EV charging, communication between vehicle and charger, and DC fast charging infrastructure. The following approach summarizes how the proposed architecture meets the existing requirements to meet IEC 61851 (conductive charging requirements), ISO 15118 (vehicle–charger communication and authentication), and IEEE 2030.1.1 (DC fast-charging infrastructure), citing design margins and acceptance criteria based upon quantifiable measures.

- Mapping of functional elements to standards

IEC 61851 (conductive charging): The control logic of the converter and protective elements specifies continuous monitoring of the DC-link, the protection operation for both overvoltage and overcurrent, the verification of isolation, and the sequencing of charger state and non-conductive charging for safe conductive charging. The fault isolation latency, which is under 300 µs, and derating ensure that transient excursions are eliminated prior to exceeding any leading-edge limits from the rated component limits.

ISO 15118 (communication & session management): The system architecture provides for the configuration of ISO 15118 trace analyses like energy transfer negotiation, charge-session management, and secure authentication. The real-time implementation framework DSP reserves an interface and buffer for vehicle control messages, while the recommended target latency for control-message responses ensures practical session outcomes such as ≤100 ms for non-safety critical command acknowledgments, <50 ms for session-control acknowledgments. Secure policy rollback and state logs for sessions are also included in the architecture and design to meet the requirements for electronic certificate-based authentication and charge authorization workflows.

IEEE 2030.1.1 (DC fast-charging infrastructure): The PPC topology and power-handling margins are scaled for high-power DC operation like fast charge, including transformer isolation practice, DC-link energy buffering, and thermal protections to allow constant high-power transfers along with grid-interfacing considerations such as harmonic, ripple, and transient management. Table 9 represents the engineering acceptance, verification, laboratory, and transient management.

4.9. Comparative analysis

The proposed PPO-type II PPC for efficient EV fast charging model evaluation is done by using the specified evaluation metrics. The proposed model is compared with the existing type II PPC [13] and type I PPC [14] models. This comparative evaluation is illustrated in Table 10. Table 10 demonstrates that the proposed PPO-type II PPC achieves superior performance by attaining peak efficiency (99.36%), compared to the existing type I PPC [14], which recorded peak efficiency (97.70%). Similarly, the conventional type II PPC [13], which achieved peak efficiency (99.11%), respectively. A graphical representation of peak efficiency comparisons is provided in Figure 3.

Furthermore, PPO-type II PPC is evaluated using partial power handling and compared with existing type II PPC [13], which are illustrated in the given Table 11. As observed in Table 11, the proposed PPO-type II PPC achieved effective partial power handling (12.21%) when compared to the existing type I PPC [14]. This result demonstrates that the proposed model maintained higher superiority by efficiently charging the EV vehicle.

4.10. Discussion

The main focus of this research is to enhance the efficiency of EV fast charging while minimizing thermal stress and power handling with PPO that is integrated with a type II PPC. The experimental and validation results indicate that the proposed PPO-type II PPC has significantly achieved better peak efficiency (99.36%) and partial power performance (12.21%) than the currently defined boost, R/D, resonant, and traditional type II PPC topologies. Because fully rated convectors implement converters that process total power and incur excess switching losses, the presented architecture only processes the partial power, which can significantly reduce stress on components and expenditure on operation. Traditional PPC designs have a strict control strategy that does not account for the fast-paced dynamics which is introduced by the battery SoC and load conditions; this creates inefficiencies in charging. The proposed PPO controller can adjust the phase shift angle in the converter to allow for real-time control sourced from system feedback, while modifying the MOSFET switching cycles to optimize the efficiency, safety, and speed of the system. The use of SiC MOSFETs in the phase-shifted full-bridge converter enables better thermal and electrical performance, thereby allowing for higher switching frequencies with negligible losses. Therefore, an improved method of adaptive control systems integrated with partial power processing will yield far greater robustness in given multiple topology options.

Table 9. Recommended quantitative design margins and acceptance criteria

Parameter	Recommended limit/Margin	Rationale/Acceptance test
DC-link voltage ripple (pp) seen by the battery	≤ 1.0% p–p of nominal battery voltage under steady charging; short transient allowance up to 2.0%	Measure ripple at battery terminals during nominal and step-load change, verify by oscilloscope/HIL data logger.
Output current ripple (rms/pp)	≤ 3% rms	Demonstrate acceptable battery cell heating and reduced calendar fade.
SoC estimation accuracy (model output)	RMSE ≤ 2.0% SoC across operating cycles, max error ≤ 4.0%	Validate against laboratory coulomb-counting baseline and standard drive cycle tests.
MOSFET junction temperature (Tj) operating limit	Tj ≤ 85 °C (operational); derate begins at 80 °C; emergency cutoff at 95 °C	Thermal ramp tests with temperature sensors; verify the derating algorithm reduces phase-shift duty within one control cycle.
Transformer turn-ratio safety margin	±5% physical tolerance from design ratio; peak flux headroom ≥ 20%	Verify no saturation under worst-case DC offset and transient.
Over-voltage protection threshold	TV_{dc} trip = 1.10 × V_{dc} nominal	Fault injection test and time-to-isolate measurement.
Over-current protection threshold	I trip = 1.20 × I rated with <300 µs isolation time	Bench test with current step injection.
Fault isolation latency	≤ 300 µs	Measure from detection to PWM suppression/gate drive disable.
EMI/Emissions	Meet automotive limits ≥ 25 dB margin above measured conducted emissions threshold in 150 kHz–10 MHz band	Conducted and radiated emissions testing on an anechoic chamber/HIL with an EMI probe.
Control latency & sampling	Control update ≤ 100 µs, sampling ≥ 10 kHz, inference latency ≤ 85 µs, on MCU/DSP target or ≤ 30 µs with FPGA acceleration	Profiling of compiled PPO policy on target hardware confirms with the timing analyzer.
Safety/redundancy	Critical thresholds are monitored by independent hardware comparators with dual-path and a software watchdog with persistent logs	Hardware-in-the-loop and fault injection validation.

Table 10. Comparative evaluation of the proposed PPO-type II PPC

Performance models	Peak efficiency (%)
Type I PPC [14]	97.70
Type II PPC [13]	99.11
Proposed PPO-type II PPC	99.36

Table 11. Comparative evaluation of the proposed PPO-type II PPC

Performance models	Partial power handling (%)
Type I PPC [14]	13.32
Proposed PPO-type II PPC	12.21

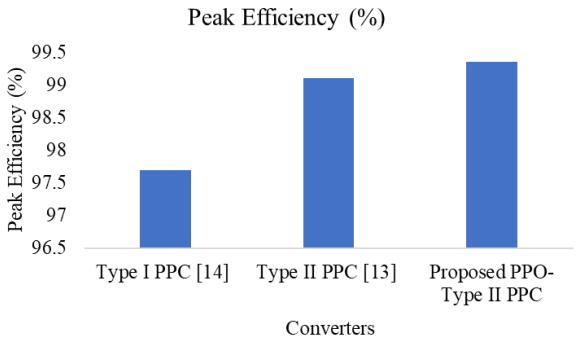

Figure 3. Shows the graphical representation of peak efficiency

5. CONCLUSION

In this research, a PPO enhanced type II PPC is employed to achieve efficient fast charging of EVs. Initially, the power from the EV charging station is passed through a low-frequency (LF) isolation transformer to ensure safe voltage level adjustment. Subsequently, an input filter is utilized to suppress high-frequency noise and maintain electromagnetic compatibility. This AC voltage is then converted into DC through a rectifier stage. From this DC voltage, a portion of the power is taken by type II PPC and the remaining power is supplied directly to the EV battery. The type II PPC is implemented using a phase-shifted full-bridge converter which incorporates four MOSFET switches and a transformer. Here, PPO continuously monitors input voltage, battery SoC and output voltage to generate the required optimal phase-shift angle (ϕ). This phase shift angle is translated into precise PWM signals that control the ON/OFF cycles of MOSFET switches. Consequently, the PPO controller enables dynamic power regulation while minimizing thermal losses and switching losses. This

accelerates the charging process and enhances system efficiency. In future, integrating the hybrid deep learning models with optimizers will efficiently generate effective phase shift angles, which will lead to a very quick charging process. Furthermore, the proposed PPO enhanced type II PPC controller will be implemented and evaluated in an environment of hardware-in-the-loop (HIL) to validate its real-time viability and control stability. The trained PPO policy will be installed on an embedded digital signal processor (DSP) like TITMS320F28379D and interfaced with a real-time simulator exchange among the virtual controller and a controller, enabling assessment of computational latency, PWM synchronization, and dynamic response under changing SoC and load conditions. This planned validation will fill the gap between physical and simulation implementation, thus enhancing the practical readiness of the proposed PPO enhanced type II PPC for further generation of EV fast charging applications.

FUNDING INFORMATION

Authors state no funding involved.

AUTHOR CONTRIBUTIONS STATEMENT

This journal uses the Contributor Roles Taxonomy (CRediT) to recognize individual author contributions, reduce authorship disputes, and facilitate collaboration.

Name of Author	C	M	So	Va	Fo	I	R	D	O	E	Vi	Su	P	Fu
Franco Aldrin Joseph Menezes	✓	✓	✓	✓	✓	✓		✓	✓	✓			✓	
Gopala Reddy Krishnappa		✓		✓		✓	✓	✓	✓	✓	✓	✓		✓

C : **C**onceptualization
M : **M**ethodology
So : **So**ftware
Va : **Va**lidation
Fo : **Fo**rmal analysis
I : **I**nvestigation
R : **R**esources
D : **D**ata Curation
O : Writing - **O**riginal Draft
E : Writing - Review & **E**diting
Vi : **Vi**sualization
Su : **Su**pervision
P : **P**roject administration
Fu : **Fu**nding acquisition

CONFLICT OF INTEREST STATEMENT

Authors state no conflict of interest.

DATA AVAILABILITY

Data sharing not applicable to this article as no dataset were generated or analyzed during the current study.

REFERENCES

[1] Y. D. Kwon, F. D. Freijedo, T. Wijekoon, and M. Liserre, "Series resonant converter-based full-bridge DC–DC partial power converter for solar pv," *IEEE Journal of Emerging and Selected Topics in Power Electronics*, vol. 12, no. 2, pp. 1719–1729, Apr. 2024, doi: 10.1109/JESTPE.2024.3355511.

[2] A. Sharida, S. Bayhan, and H. Abu-Rub, "Enhancing scalability of fast electric vehicle charging stations: solutions for AC–DC side integration and regulation," *IEEE Open Journal of the Industrial Electronics Society*, vol. 4, pp. 720–731, 2023, doi: 10.1109/OJIES.2023.3349094.

[3] N. Yadav *et al.*, "Performance evaluation of step-up/down partial power converters based on current-fed DC-DC topologies," *IEEE Transactions on Industry Applications*, vol. 60, no. 5, pp. 7111–7124, Sep. 2024, doi: 10.1109/TIA.2024.3413050.

[4] S. Mönch *et al.*, "A 99.74% efficient capacitor-charging converter using partial power processing for electrocaloric," *IEEE Journal of Emerging and Selected Topics in Power Electronics*, vol. 11, no. 4, pp. 4491–4507, Aug. 2023, doi: 10.1109/JESTPE.2023.3270375.

[5] N. Hassanpour, A. Chub, A. Blinov, and D. Vinnikov, "Soft-switching bidirectional step-up/down partial power converter with reduced components stress," *IEEE Transactions on Power Electronics*, vol. 38, no. 11, pp. 14166–14177, 2023, doi: 10.1109/TPEL.2023.3289061.

[6] K. Momoh, S. A. Zulkifli, P. Korba, F. R. S. Sevilla, A. N. Afandi, and A. Velazquez-Ibañez, "State-of-the-art grid stability improvement techniques for electric vehicle fast-charging stations for future outlooks," *Energies*, vol. 16, no. 9, p. 3956, May 2023, doi: 10.3390/en16093956.

[7] C. Chatterjee, A. F. Khan, and S. S. Nag, "A bidirectional three-phase unfolding based high efficiency EV charger featuring partial power operation," in *2024 Energy Conversion Congress & Expo Europe (ECCE Europe)*, IEEE, 2024, pp. 1–8, doi: 10.1109/ECCEEurope62508.2024.10751903.

[8] S. Gao, Y. Zhang, Y. Wang, J. Liu, and D. Xu, "An optimal control strategy for the dab-based partial power converter based on extended-phase-shift control," *IEEE Open Journal of Power Electronics*, vol. 4, pp. 817–827, 2023, doi: 10.1109/OJPEL.2023.3319488.

[9] Y. D. Kwon, F. D. Freijedo, T. Wijekoon, and M. Liserre, "A multiport partial power converter for smart home applications," *IEEE Transactions on Power Electronics*, vol. 39, no. 7, pp. 8824–8833, Jul. 2024, doi: 10.1109/TPEL.2024.3388322.

[10] J. Anzola, A. Arruti, I. Aizpuru, E. Agirrezabala, and M. Mazuela, "50 kW partial power converter for EV charging," in *2024 Energy Conversion Congress & Expo Europe (ECCE Europe)*, IEEE, Sep. 2024, pp. 1–8. doi: 10.1109/ECCEEurope62508.2024.10751828.
[11] F. Kaya and O. Akar, "Short circuit effects on HV feeders of optimally located electric vehicle fast charging stations," *IEEE Access*, vol. 12, pp. 47842–47853, 2024, doi: 10.1109/ACCESS.2024.3383433.
[12] L. Zhu, H. Bai, and A. Brown, "Model and control of a current-fed dual active bridge based ultrawide-voltage-range auxiliary power module for 400 V/800 V electric vehicles," *IEEE Transactions on Power Electronics*, vol. 39, no. 3, pp. 3263–3276, Mar. 2024, doi: 10.1109/TPEL.2023.3337712.
[13] S. Rivera *et al.*, "Partial-power converter topology of type ii for efficient electric vehicle fast charging," *IEEE Journal of Emerging and Selected Topics in Power Electronics*, vol. 10, no. 6, pp. 7839–7848, Dec. 2022, doi: 10.1109/JESTPE.2021.3117910.
[14] D. Pesantez, H. Renaudineau, S. Rivera, A. Peralta, A. Marquez Alcaide, and S. Kouro, "Transformerless partial power converter topology for electric vehicle fast charge," *IET Power Electronics*, vol. 17, no. 8, pp. 970–982, 2024, doi: 10.1049/pel2.12613.
[15] C. A. F. D. Freitas, P. Bartholomeus, X. Margueron, and P. Le Moigne, "Partial power converter for electric vehicle hybrid energy storage system using a controlled current source cascade architecture," *IEEE Access*, vol. 12, pp. 150898–150913, 2024, doi: 10.1109/ACCESS.2024.3477935.
[16] V. Ramya and R. Marimuthu, "Integration of AC/DC with multi input mode selection converter for fast charging of battery in electric vehicles," *IEEE Access*, vol. 12, pp. 127115–127126, 2024, doi: 10.1109/ACCESS.2024.3456472.
[17] M. A. Elkeiy, Y. N. Abdelaziz, M. S. Hamad, A. S. Abdel-Khalik, and M. Abdelrahem, "Multiport dc-dc converter with differential power processing for fast EV charging stations," *Sustainability (Switzerland)*, vol. 15, no. 4, 2023, doi: 10.3390/su15043026.
[18] D. Elizondo-Martinez, E. L. Barrios, M. Galdeano, A. Ursua, and P. Sanchis, "Novel two-stage three-level converter with inherently balanced DC voltage for EV fast-charging applications," *IEEE Transactions on Transportation Electrification*, vol. 10, no. 3, pp. 6418–6433, 2024, doi: 10.1109/TTE.2023.3339583.
[19] R. V. Jyothsna, A. A. Dar, S. Kadam, and V. M. Iyer, "Non-isolated partial power processing converter for battery energy storage systems," in *2024 IEEE International Communications Energy Conference (INTELEC)*, IEEE, Aug. 2024, pp. 1–6. doi: 10.1109/INTELEC60315.2024.10679021.
[20] N. G. F. Dos Santos, A. Toebe, P. H. B. Löbler, L. Schuch, M. L. D. S. Martins, and C. Rech, "A high-efficient single-switch switched-capacitor partial power converter for on-board chargers," *IEEE Transactions on Power Electronics*, vol. 39, no. 11, pp. 15269–15280, Nov. 2024, doi: 10.1109/TPEL.2024.3443519.
[21] R. Wei, L. Ding, and Y. Li, "Efficiency-oriented optimized design and control of hybrid FSBB– CLLC converters with partial power processing capability," *IEEE Transactions on Power Electronics*, vol. 39, no. 5, pp. 6364–6375, May 2024, doi: 10.1109/TPEL.2024.3363629.
[22] P. Le Métayer, Q. Loeuillet, F. Wallart, C. Buttay, D. Dujic, and P. Dworakowski, "Phase-shifted full bridge DC–DC converter for photovoltaic MVDC power collection networks," *IEEE Access*, vol. 11, pp. 19039–19048, 2023, doi: 10.1109/ACCESS.2023.3247952.
[23] N. Yadav, N. Hassanpour, A. Chub, A. Blinov, and D. Vinnikov, "Improved maximum power point tracking algorithm for step-up/down partial power converters operating around zero partiality," *IEEE Journal of Emerging and Selected Topics in Power Electronics*, vol. 12, no. 2, pp. 1984–1994, Apr. 2024, doi: 10.1109/JESTPE.2024.3354843.
[24] Y. Tian, Y. Li, B. Cao, F. Wei, and Y. Zheng, "Systematic topology synthesis and power density visualization of partial power processing architecture," *IEEE Transactions on Power Electronics*, vol. 40, no. 1, pp. 1346–1358, 2025, doi: 10.1109/TPEL.2024.3446997.
[25] A. K. Singh, M. A. Chaudhari, K. S. R. Sekhar, and R. Kumar, "Analysis of isolated dc-dc converters for electric-vehicle (EV) battery charging," *2023 IEEE Renewable Energy and Sustainable E-Mobility Conference, RESEM 2023*, 2023, doi: 10.1109/RESEM57584.2023.10236354.

BIOGRAPHIES OF AUTHORS

Franco Aldrin Joseph Menezes has served as an assistant professor in the Department of Electrical and Electronics Engineering at St Joseph Engineering College, Mangaluru, since 2009. He holds a bachelor's degree in electrical and electronics engineering and a master's degree in power electronics, both from Visvesvaraya Technological University (VTU), and is currently pursuing his Ph.D. from VTU. He has guided several student projects, with a number of them receiving funding from the Karnataka State Council for Science and Technology (KSCST). He has also contributed to the Journal of Engineering Education Transformations and has presented research papers at international conferences. Before joining academia, he worked as an associate IT Consultant at ITC Infotech. His areas of interest include power electronics, embedded systems, and student mentorship. He remains committed to academic excellence, research, and the holistic development of students at the institution. He can be contacted at email: aldrinmenezes@gmail.com.

Gopala Reddy Krishnappa is a professor and head of the Department of Electrical and Electronics Engineering at Vidyavardhaka College of Engineering (VVCE), Mysuru, Karnataka, India. He earned his Ph.D. from Visvesvaraya Technological University in 2019 and has been serving at VVCE since 2007. His research interests encompass power systems and electrical machines. He has contributed to the field through publications in journals and conference proceedings. He led a project titled "Solar Powered Landmine Detection Robotic Vehicle with GPS Positioning," funded by the Karnataka State Council for Science and Technology (KSCST). He holds lifetime memberships in the Indian Society for Technical Education and the Institution of Engineers (India). His dedication to teaching and research significantly contributes to the advancement of electrical engineering education and innovation. He can be contacted at email: gopal.reddy@vvce.ac.in.